CAN HIGHER-ORDER STATISTICS ADD INFORMATION IN MODEL-BASED POLARIMETRIC DECOMPOSITIONS?

Anthony P. Doulgeris and Torbjørn Eltoft

University of Tromsø -The Arctic University of Norway, 9037 Tromsø, Norway

anthony.p.doulgeris@uit.no, torbjorn.eltoft@uit.no

ABSTRACT

This work details how to obtain additional information to find a unique solution to model-based polarimetric decompositions. In general, polarimetric target decomposition methods decompose the multi-look covariance or coherency matrix, a second-order statistic, into a mixture of components. These complex matrices only have five distinct elements that equates to five distinct expressions for the model-based decomposition. However, virtually all models involve more than five physical parameters, making the decomposition underdetermined and hence does not have a single unique solution. The general approach to solve this problem is to make certain assumptions, thus fixing one or more parameters, allowing the other free parameters to be solved from the set of expressions. This work describes how to obtain new, independent expressions from higher order statistical moments to obtain a unique solution and presents preliminary results.

Key words: Polarimetric Decomposition; Product Model; Scattering mechanisms, Statistics.

1. INTRODUCTION

The backscatter of SAR signals from Arctic sea ice, and many other rough surfaces, is thought to be caused by a combination of several scattering mechanisms, in general categorised as surface scattering, volume scattering, and double bounce scattering. SAR polarimetry has the capability of decomposing the signals into components representing these specific mechanisms. One class of polarimetric decomposition theorems is denoted model-based decompositions, in which, a physical model is connected to the various scattering mechanisms. The Freeman-Durden three-component model [1] is a well-known example of a model-based decomposition algorithm, where a specific parameterised model is associated with the covariance matrix of each of the above-mentioned components. There is experimental evidence that electromagnetic backscatter from sea ice in some cases has a high degree of depolarisation. Depolarisation is in some decomposition models mostly attributed to volume scattering. However, for sea ice backscattering it is anticipated that depolarisation can also be caused by surface effects related to rough and highly deformed ice, as well as by volume type scattering from brine inclusions and inhomogeneities inside the ice column.

Previous analysis of polarimetric decompositions of sea ice scenes using existing algorithms show that the power of the double bounce component often is an order of magnitude below the contribution from surface and volume scattering, and that high double bounce is restricted to isolated features [2]. Hence, we will in this study explore model-based polarimetric decomposition using a model which consists of only two terms; a surface scattering component and a volume scattering component. The surface component is to be described by the extended Bragg (X-Bragg) model [3], which can also predict surface based depolarisation. The volume component is modelled as an azimuth symmetric scattering mechanism, consisting of randomly oriented scatterers, geometrically categorised with a single shape parameter. In total, the model for the polarimetric coherence matrix has 6 unknowns, but only 5 independent equations to solve for the parameters. Hence, the system is underdetermined (like many decomposition models).

In this paper we explore how higher-order statistical moments can add information, and be used to obtain a determined set of equations. We will both discuss theoretical aspects of our methodology, and show results of preliminary studies based on simulated and real data.

2. BASIC APPROACH

Traditional Decompositions model the covariance or coherency matrix as a mixture of contributions

$$\mathbf{C} = \sum_{j=1}^{N_c} P_j \tilde{\mathbf{C}}_j \qquad \text{or} \qquad \mathbf{T} = \sum_{j=1}^{N_c} P_j \tilde{\mathbf{T}}_j$$

where P_j represents the power in each component and $\tilde{\mathbf{C}}_j$ or $\tilde{\mathbf{T}}_j$ are SPAN normalised covariance or coherency matrices for each scattering model.

For example, the Freeman-Durden 3-component decomposition [1] looks like

$$\mathbf{C} = P_s\tilde{\mathbf{C}}_s + P_d\tilde{\mathbf{C}}_d + P_v\tilde{\mathbf{C}}_v$$

with single-bounce, double-bounce and volume components.

Under such modelling the P_js are independent variables in the solution and there is one for each component N_c, e.g., 3 for Freeman-Durden. It is equivalent to convert to power fractions, such that

$$f_j = P_j/\text{SPAN} \qquad \text{or} \qquad P_j = f_j\,\text{SPAN}$$

Hence, Freeman-Durden becomes

$$\mathbf{C} = f_s\,\text{SPAN}\,\tilde{\mathbf{C}}_s + f_d\,\text{SPAN}\,\tilde{\mathbf{C}}_d + f_v\,\text{SPAN}\,\tilde{\mathbf{C}}_v$$

There are still N_c independent variables, SPAN + $(N_c - 1)$ fractions due to the constraint $\sum_{j=1}^{N_c} f_j = 1$.

Thinking about decompositions as mixing fractions leads to a statistical interpretation as a probabilistic mixture with the implication that we may carry this mixture modelling down to the the scattering vector level ($\mathbf{s}$ or $\mathbf{k}$) as, for example,

$$p_k(\mathbf{k}) = \sum_{j=1}^{N_c} f_j\, p_j(\mathbf{k}) \tag{1}$$

Note: this may not be the only way to mix components, but it is our first approach with solid statistical properties.

The consequence of (1) is that the second order statistics are exactly as before

$$\mathbf{T} = \sum_{j=1}^{N_c} f_j\,\text{SPAN}\,\tilde{\mathbf{T}}_j$$

Additionally, for each channel i, i.e., vector dimension k_i, we have

$$E\{|k_i|^2\} = \sum_{j=1}^{N_c} f_j\,\text{SPAN}\,\tilde{T}_{ii,j}$$

where $\tilde{T}_{ii,j}$ is the i^{th} diagonal elements of the j^{th} model matrix.

Furthermore, let us consider the scalar product model for texture, such that

$$k_i = \sqrt{\tau_j}\,X_{i,j}\ ;\ X_{i,j} \sim \mathcal{N}_1^c(0,1) \text{ and } E\{\tau_j\} = 1$$

Then, it follows that the fourth order statistic in each channel is

$$E\{|\mathbf{k}_i|^4\} = \sum_{j=1}^{N_c} f_j\, 2\, E\{\tau_j^2\}\,\text{SPAN}^2\,\tilde{T}_{ii,j}^2 \tag{2}$$

These are unique equations and valid for any scattering component models. Note that if we assume no texture, i.e., Gaussian vectors, then $E\{\tau_j^2\} = 1$.

3. AN EXAMPLE DECOMPOSITION

We shall explore the two component X-Bragg model for sea ice that we have introduced before [2].

$$\begin{aligned}
\tilde{\mathbf{T}} &= f_s\,\text{SPAN}\,\tilde{\mathbf{T}}_s + (1-f_s)\,\text{SPAN}\,\tilde{\mathbf{T}}_v \\
\tilde{\mathbf{T}}_s &= \frac{1}{(1+|\beta|^2)}\begin{bmatrix} 1 & \beta^*\text{sinc}(2\delta) & 0 \\ \beta\text{sinc}(2\delta) & \frac{1}{2}|\beta|^2(1+\text{sinc}(4\delta)) & 0 \\ 0 & 0 & \frac{1}{2}|\beta|^2(1-\text{sinc}(4\delta)) \end{bmatrix} \\
\tilde{\mathbf{T}}_v &= \frac{1}{(3-\rho)}\begin{bmatrix} 1+\rho & 0 & 0 \\ 0 & 1-\rho & 0 \\ 0 & 0 & 1-\rho \end{bmatrix}
\end{aligned}$$

This model has six parameters (f_s, SPAN, δ, and ρ real, plus β complex), but only five equations (3 real diagonals, plus one complex off-diagonal). The physical parameters have the following definitions:

$$\begin{aligned}
\beta &= \frac{R_{hh} - R_{vv}}{R_{hh} + R_{vv}} \\
R_{hh} &= \frac{\cos(\theta) - \sqrt{\varepsilon - \sin^2(\theta)}}{\cos(\theta) + \sqrt{\varepsilon - \sin^2(\theta)}} \\
R_{vv} &= \frac{(\varepsilon-1)(\sin^2(\theta) - \varepsilon(1+\sin^2(\theta)))}{\cos(\theta) + \sqrt{\varepsilon - \sin^2(\theta)}} \\
\theta &= \text{incidence angle} \\
\varepsilon &= \text{complex permittivity} \\
\delta &= \text{X-Bragg slope variation angle} \\
\rho &= \text{ellipsoidal shape parameter}
\end{aligned}$$

Table 1 depicts the full set of equations for the decomposition, the first ones based on the second-order coherency matrix $\mathbf{T}$ alone, to which the fourth-order expressions are added. If we take the simple case with Gaussian component scattering vectors, then the equations can be solved analytically and are very fast to evaluate. Note that we have not yet accounted for the speckle variation in any way. We chose a large number of looks to avoid too much variation, and we expect that the analytical solution will possibly produce the occasional invalid solution. To overcome this and for the case with unknown radar texture, i.e., non-unity moments for τ, we suggest some form of non-linear error function minimisation routine.

4. PRELIMINARY RESULTS

We built a coherency matrix test-pattern, with 6×6 blocks, with different parameter values within the valid range of parameter values for sea ice and ocean properties. We generated data for each block of 200×200 pixels for this simulated test-pattern by a 'hard' probabilistic mixture model for the scattering vectors under

$$p_k(\mathbf{k}) = \sum_{j=1}^{N_c} f_j\,\mathcal{N}_d^c(\mathbf{0}; \tilde{\mathbf{T}}_j)$$

Table 1. The full set of equations for our two-component sea ice decomposition example.

The second-order expressions

$$
\begin{aligned}
< T_{11} > &= f_s \,\text{SPAN}\, \frac{1}{(1+|\beta|^2)} + (1-f_s)\,\text{SPAN}\, \frac{(1+\rho)}{(3-\rho)} \\
< T_{22} > &= f_s \,\text{SPAN}\, \frac{|\beta|^2(1+\text{sinc}(4\delta))}{2(1+|\beta|^2)} + (1-f_s)\,\text{SPAN}\, \frac{(1-\rho)}{(3-\rho)} \\
< T_{33} > &= f_s \,\text{SPAN}\, \frac{|\beta|^2(1-\text{sinc}(4\delta))}{2(1+|\beta|^2)} + (1-f_s)\,\text{SPAN}\, \frac{(1-\rho)}{(3-\rho)} \\
< T_{12} > &= f_s \,\text{SPAN}\, \frac{\beta^*(\text{sinc}(2\delta))}{(1+|\beta|^2)}
\end{aligned}
$$

The fourth-order expressions

$$
\begin{aligned}
< k_1^{(4)} > &= 2\,E\{\tau^2\}\,\text{SPAN}^2 \left(f_s \left[\frac{1}{(1+|\beta|^2)}\right]^2 + (1-f_s)\left[\frac{(1+\rho)}{(3-\rho)}\right]^2 \right) \\
< k_2^{(4)} > &= 2\,E\{\tau^2\}\,\text{SPAN}^2 \left(f_s \left[\frac{|\beta|^2(1+\text{sinc}(4\delta))}{2(1+|\beta|^2)}\right]^2 + (1-f_s)\left[\frac{(1-\rho)}{(3-\rho)}\right]^2 \right) \\
< k_3^{(4)} > &= 2\,E\{\tau^2\}\,\text{SPAN}^2 \left(f_s \left[\frac{|\beta|^2(1-\text{sinc}(4\delta))}{2(1+|\beta|^2)}\right]^2 + (1-f_s)\left[\frac{(1-\rho)}{(3-\rho)}\right]^2 \right)
\end{aligned}
$$

with the multivariate complex Gaussian data model. We then used a large number of looks, for example 50×50, to suppress the speckle variation and to get the right mixtures on average for the multi-look coherency matrix image, under our modelling assumptions. The fourth-order moments were calculated from the SLC scattering vectors for each dimension within each multi-look window. Finally, we use the decomposition to try to recover the parameters and compare to the original generated values.

An example of the generated image is shown as a Pauli RGB image in Fig. 1 and the results for this test-pattern are shown in Fig. 2. The first row of Fig. 2(a) shows five of the physical parameters (f_s, f_v, δ, ρ and $|\beta|^2$), and can be visualised as the colour reference for the quality of the results since we keep all the colour scales fixed. The second row (b) shows our previous results when using only the second-order statistics, and although many of the features are quite well recovered, the last $|\beta|^2$ image is quite flat. We have found that the $|\beta|^2$ image stays essentially close to the initialising search value, because there are not enough equations to fix this parameter uniquely. Fig. 2(c) shows the newly proposed results adding the fourth-order equations and clearly recovers all the parameters much better than before. We see the occasional random solution, which we expect is due to not accounting for the speckle induced error in the solution. In particular, the extra equations have allowed us to determine the last $|\beta|^2$ image that was not determined previously.

Since the solution was assuming the the components were Gaussian, we also did a quick test where we generated non-Gaussian components, with an K-distribution with

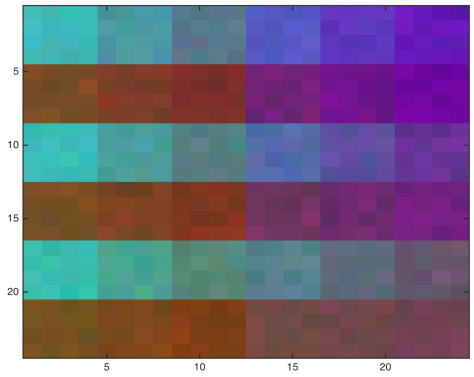

Figure 1. Pauli RGB image of test-pattern, showing the block-wise parameter variation and slight remaining speckle variation after 50×50 *mulit-looking.*

moderate texture ($\alpha = 10$), but still used the Gaussian-based analytical solution (since we have not yet implemented a non-Gaussian approach). See Fig. 2(d). What we see is that the solution is still generally correct, but that the extra non-Gaussian variance leads to an over-estimation in the physical parameters.

The final experiment is with real sea ice data from a Radarsat-2 scene of the Fram strait from Septemeber 2011. The Pauli RGB image and the resulting extracted physical parameter images are shown in Fig. 3. The scene depicts some open water, some smooth level ice, some rough deformed ice areas, and some ridges. In addition, we have information from a helicopter-borne laser altimeter that confirms that the pink central shape is smooth, while the upper and lower areas are very rough deformed ice. Interpreting the five physical parameter images, we can clearly see that many known physical relations are correctly modelled. Some examples follow.

The open water is dominantly surface scattering, and low volume scattering, as expected. There appears to be a small region of low-surface high-volume scattering mechanisms near the top-right corner that we suspect from other studies to be multi-year ice or an iceberg. The open water and the central smooth ice area have very low delta parameter, which describes the degree of roughness of the X-Bragg model, as would be expected. The rough ice and in particular the ridges have the highest delta value. The open water has the highest B2 values, which corresponds to highest dielectric properties, as expected, while the ridges seem to have quite high values also, but this may be due the the known texture induced over-estimation that we demonstrated in the simulated experiments. The rho value is harder to interpret, but depicts dipole shaped random scatterers in the ridges, while more elliptical and circular elsewhere.

5. CONCLUSIONS

This is only the preliminary results, but it already looks promising for real world data. We have clearly demonstrated our main objective, which answers our title question in the affirmative. Yes, higher order statistics can add value to solving model-based decompositions.

We have a fast algebraic solution for Gaussian scattering vector components, but have not yet solved the equations for textured data. However, since we have several extra equations, we see no reason why this cannot be achieved, if not analytically solved, then through an error function minimisation.

In addition, such a minimisation should also reduce some of the invalid solutions due to the additional speckle variation that is not currently accounted for.

The modelling appears to give realistic results for a real sea ice data-set, but has not yet been validated to the actual dielectric parameters, or correlated to the helicopter-borne surface roughness measurements.

The derived high-order statistical expressions are found to be independent of the actual physical model, and relate back to the second-order covariance or coherency matrices only. Hence, we believe that this approach should add value to all underdetermined decomposition schemes and this shall be tested for other decompositions in the future.

Finally, we still have to confirm that this is an appropriate mixing model for target decompositions at the scattering level, but the initial real world interpretation results makes this quite likely.

REFERENCES

[1] A. Freeman and S. L. Durden. A Three-Component Scattering model for Polarimetric SAR Data. *IEEE Transactions on Geoscience and Remote Sensing*, 36, 3:963–973, May 1998.

[2] A.P. Doulgeris Eltoft, T and J. Grahn. Model-based polarimetric decomposition of arctic sea ice. In *Proc. EUSAR 2014 – 10th European Conference on Synthetic Aperture Radar*, Berlin, Germany, pages 822–825, June 2014.

[3] I. Hajnsek, E. Pottier, and S.R. Cloude. Inversion of surface parameters from polarimetric sar. *Geoscience and Remote Sensing, IEEE Transactions on*, 41(4):727–744, April 2003.

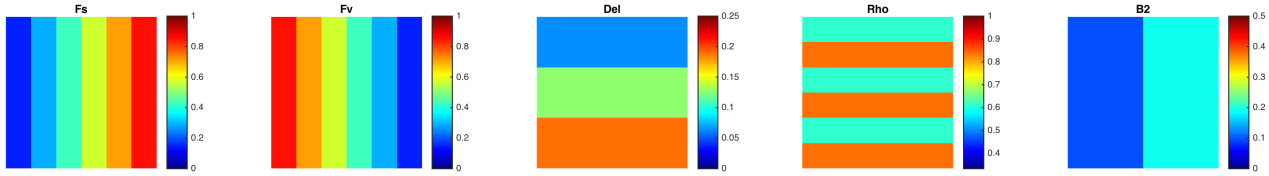

(a) Ground Truth images (fixed scales, colour reference)

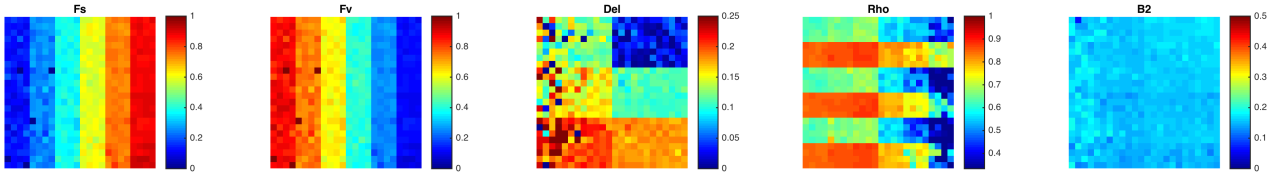

(b) Recovered parameters, with second-order only (free search)

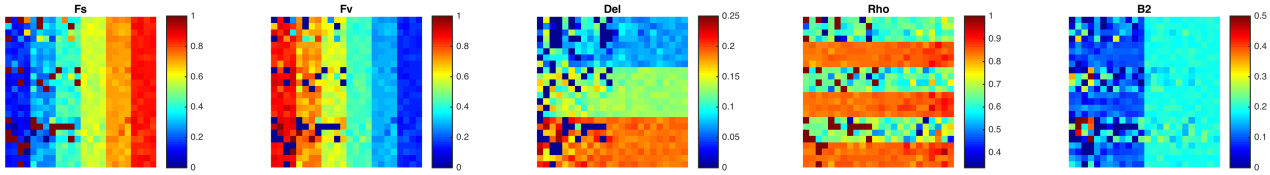

(c) Recovered with fourth-order (Gaussian, algebraic solution)

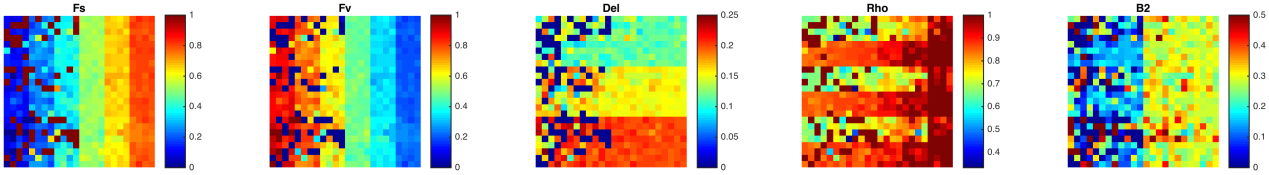

(d) Non-Gaussian ($\alpha = 10$) generated data (Gaussian solution)

Figure 2. Preliminary results for the simulated test-pattern under different test conditions. The colour scale is fixed for all plots to give an immediate visual validation, and the columns represent different physical parameters. The generated and expected values on the top, followed by the previous second-order only results, the proposed higher-order solution results, and a non-Gaussian experiment at the bottom.

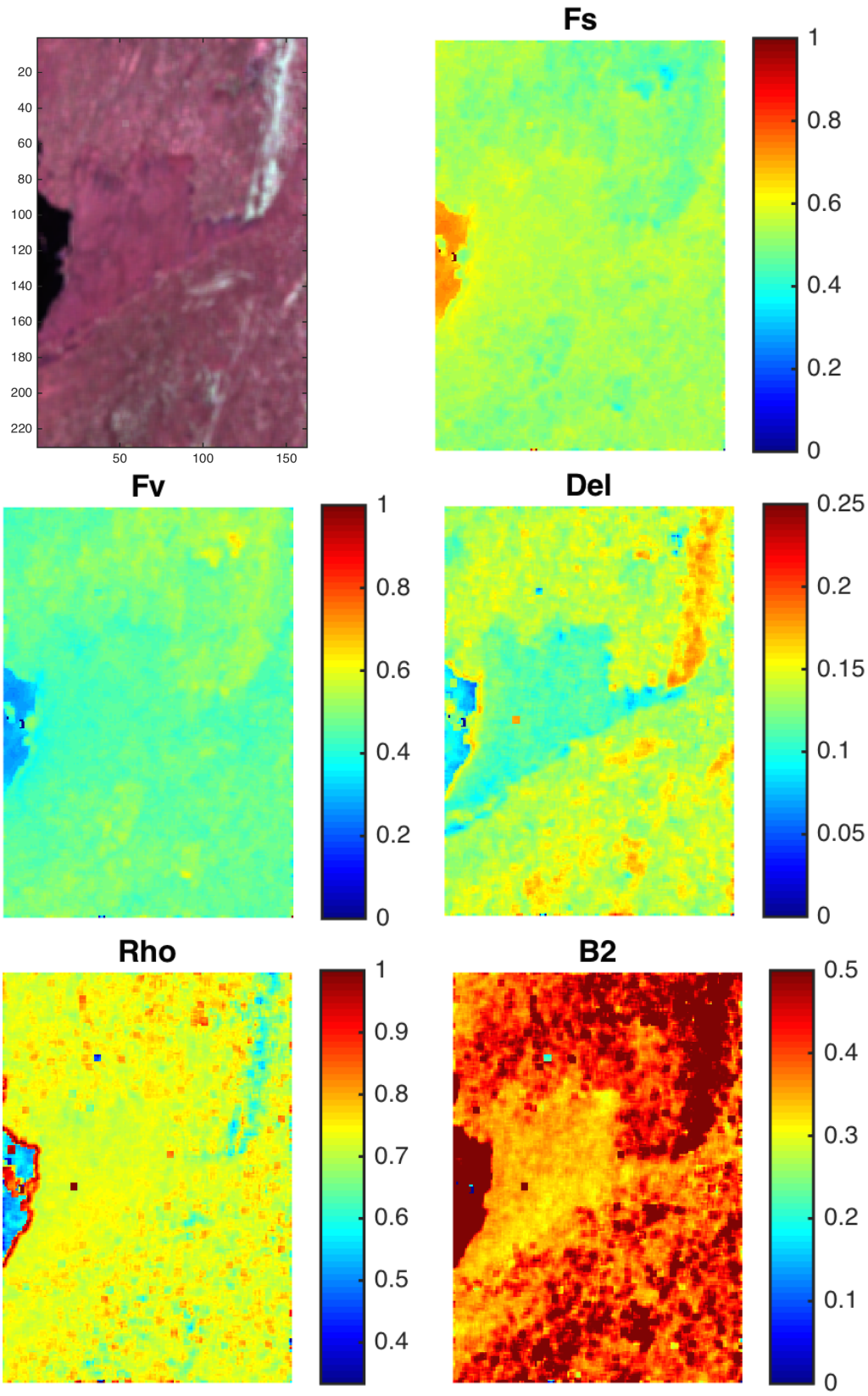

Figure 3. Real Sea Ice image, Pauli RGB (top-left), 50×50 *multi-looking. The other images show the respective physical parameter values for interpretation and does appear to capture the correct physical relations.*